

Even-Numbered Metal Chain Complexes: Synthesis, Characterization, and DFT Analysis of $[\text{Ni}_4(\mu_4\text{-Tsdpda})_4(\text{H}_2\text{O})_2]$ ($\text{Tsdpda}^{2-} = N\text{-}(p\text{-toluenesulfonyl})\text{dipyridyldiamido}$), $[\text{Ni}_4(\mu_4\text{-Tsdpda})_4]^+$, and Related Ni_4 String Complexes

Xavier López,^{*†} Ming-Yi Huang,[‡] Gin-Chen Huang,[‡] Shie-Ming Peng,^{*‡} Feng-Yin Li,^{‡§} Marc Bénard,[†] and Marie-Madeleine Rohmer[†]

Laboratoire de Chimie Quantique, Institut de Chimie, LC3-UMR 7177, CNRS-ULP, Strasbourg, France, and the Department of Chemistry, National Taiwan University, Taipei 10764, Taiwan, Republic of China

Received July 6, 2006

The synthesis and the X-ray structure of two complexes exhibiting a linear chain of four nickel atoms is reported, following $\text{Ni}_4(\mu_4\text{-phdpda})_4$ (**1**), which had been characterized previously. $[\text{Ni}_4(\mu_4\text{-Tsdpda})_4(\text{H}_2\text{O})_2]$, where H_2Tsdpda is $N\text{-}(p\text{-toluenesulfonyl})\text{dipyridyldiamine}$ (**2**), is axially coordinated to two water molecules, at variance with **1**. One-electron oxidation of **2** resulted in the loss of the axial ligands, yielding $[\text{Ni}_4(\mu_4\text{-Tsdpda})_4]^+$, [**3**]⁺, which was also structurally characterized. Finally, we report the structure of $\text{Ni}_4(\mu_4\text{-DAniDANY})_4$ (**4**), a complex synthesized starting from the new ligand N,N' -bis- p -anisyl-2,7-diamino-1,8-naphthyridine. Magnetic measurements concluded that **4** is diamagnetic, like **1**, whereas **2** is antiferromagnetic ($-2J_{14} = 80 \text{ cm}^{-1}$, using the Heisenberg Hamiltonian $\hat{H} = -2J_{14} \hat{S}_1 \cdot \hat{S}_4$), as are other axially coordinated chains with an odd number of nickel atoms. DFT calculations are reported on these complexes in order to rationalize their electronic structure and their magnetic behavior. The magnetic properties of the $[\text{Ni}_4]^{8+}$ complexes are governed by the electronic state of the Ni^{II} atoms, which may be either low-spin ($S = 0$), or high-spin ($S = 1$). DFT calculations show that the promotion to high spin of two Ni atoms in the chain, either external or internal, depends on the interplay between axial and equatorial coordination. The synergy between axial coordination and the presence of electron-withdrawing toluenesulfonyl substituents in **2** favors the promotion to the high-spin state of the terminal Ni atoms, thus yielding an antiferromagnetic ground state for the complex. This is at variance with complexes **1** and **4**, for which the lowest quintet state results from the promotion to high spin of the internal nickel atoms, together with an important ligand participation, and is destabilized by 9 to 16 kcal mol⁻¹ with respect to the diamagnetic ground state.

Introduction

The control gained in the past decade over the synthesis of $\text{C}_5\text{H}_4\text{N}(\text{NHC}_5\text{H}_3\text{N})_n\text{NHC}_5\text{H}_4\text{N}$ polypyridylamine molecules with definite values of n between 0 and 3 and beyond and the use of their deprotonated counterparts as ligands have opened a route toward the synthesis and the characterization of a new family of 1D transition-metal complexes. These

complexes are made of the assembly of four polypyridylamide molecules with a given value of n ($n\text{-ppa}$), spiraling around a framework composed of $2n + 3$ transition metal atoms in a linear arrangement.¹ The possibility to synthesize such complexes with various transition metals, mainly belonging to the first transition row ($\text{M} = \text{Cr}, \text{Co}, \text{Ni}, \text{Cu}$),¹ but also to the second one (Rh, Ru),² and the possibility to extend the metal framework with a variety of anionic ligands

* Corresponding authors. X.L.: current address, Depart. de Química Física i Inorganica, Universitat Rovira i Virgili, Campus Sescelades, c.Marcel·lí-Domingo s/n, Tarragona 43007, Spain; E-mail, javier.lopez@urv.net (X.L.); smpeng@tu.edu.tw (S.-M.P.).

† CNRS-ULP.

‡ National Taiwan University.

§ Current address: Department of Chemistry, National Chung Hsing University, Taichung, Taiwan.

(1) (a) Berry, J. F. In *Multiple Bonds between Metal Atoms*, 3rd ed.; Cotton, F. A., Murillo, C. A., Walton, R. A., Eds.; Springer-Science and Business Media, Inc.: New York, 2005. (b) Bera, J. K.; Dunbar, K. R. *Angew. Chem., Int. Ed.* **2002**, *41*, 4453. (c) Zhu, L.-G.; Peng, S.-M. *Wuji Huaxue Xuebao* **2002**, *18*, 117. (d) Yeh, C.-Y.; Wang, C.-C.; Chen, C.-H.; Peng, S.-M.; In *Redox Systems Under Nano-Space Control*; Hirao, T., Ed.; Springer-Verlag: Berlin, 2006.

in axial position³ have categorized this family as the prototype of the so-called extended metal atom chains (EMACs).⁴ The vast majority of EMACs belonging to this family involve an odd number of metal atoms, due to the very nature of *n*-polypyridylamine molecules, which give rise upon deprotonation to $(2n + 3)$ -dentate ligands. Most comparative studies compiling the structural and magnetic properties of such complexes with variable lengths are therefore restricted to $M_{2n+3}(n\text{-ppa})_4L_2$, with $n_{\text{max}} = 1$ for Co,⁵ 2 for Cr,⁶ and 3 for Ni.⁷ On the theoretical side, most nonempirical studies carried out to date for delineating correlations between the electronic structure and the geometrical and magnetic properties have been focused on $M_3(\text{dpa})_4L_2$ systems, where dpa (Hdpa = dipyridylamine) is the standard ligand corresponding to $n = 0$.^{8,9} However, two recent theoretical works have approached the problem of higher nuclearity string complexes $M_{2n+3}(\mu\text{-ppa})_4Cl_2$, either with $M = \text{Cr}$, $n = 0\text{--}2$ ¹⁰ or with $M = \text{Ni}$ and $n = 1, 2$.¹¹ Reports on ppa-based EMACs involving an *even number* of metal atoms remain extremely scarce, since they require the synthesis of new, $(2n + 4)$ -dentate ligands derived from the classical *n*-ppa molecule. Two such complexes have been characterized to date. On one hand, Cotton et al have employed the anion of bis(2-pyridyl)formamidine, DpyF^- , as a ligand for the synthesis of the dianion $[\text{Cr}_4(\text{DpyF})_4\text{Cl}_2]^{2-}$ in which the linear chain of Cr atoms is formed of two short outer bonds (2.01 Å) separated by a long inner Cr...Cr distance (2.73 Å).¹² On the other hand, Peng et al have grafted a phenylamine substituent to a standard Hbromodpa molecule, thus generating *N*-phenyldipyridyldiamine

(H_2phdpda). When deprotonated, this molecule was used as a tetradentate ligand to synthesize $\text{Ni}_4(\mu_4\text{-phdpda})_4$ (**1**), an axially uncoordinated neutral complex exhibiting the usual helical wrapping of ppa ligands around the linear metal chain.¹³ The central Ni–Ni distance is slightly shorter than the outer ones and, at variance with the whole sequence of $\text{Ni}_{2n+3}(n\text{-ppa})_4\text{Cl}_2$ metal chains, the tetranickel complex is diamagnetic.¹³ In the present work, *p*-toluenesulfonyl chloride was grafted to dipyridyldiamine (H_3dpda). Treatment of the resulting *N*-(*p*-toluenesulfonyl)dipyridyldiamine (H_2Tsdpda) with $\text{Ni}(\text{OAc})_2 \cdot 4\text{H}_2\text{O}$ resulted in the synthesis of $[\text{Ni}_4(\mu_4\text{-Tsdpda})_4(\text{H}_2\text{O})_2]$ (**2**), an axially coordinated $(\text{Ni}_4)^{8+}$ complex whose magnetic properties differ from those of **1**. Oxidation of **2** resulted in the removal of the axial water ligands, yielding $[\text{Ni}_4(\mu_4\text{-Tsdpda})_4]^+$, [**3**]⁺, and providing a first opportunity to investigate the role of axial coordination in a particular chain complex with an even number of metal atoms. The tetradentate ligand DAniDANy, with $\text{H}_2\text{-DAniDANy} = N,N'$ -bis-*p*-anisyl-2,7-diamino-1,8-naphthyridine, was also used to stabilize a tetranuclear nickel string complex, $[\text{Ni}_4(\mu_4\text{-DAniDANy})_4]$ (**4**, Figure 1). We report the structural characterization of **2**, [**3**]⁺, and **4**, along with the magnetic behavior of these complexes. A theoretical investigation was carried out at the DFT level on the model compounds **1'**, **2'**, **3'**, and [**3'**]⁺, in which the phenyl and tolyl substituents have been replaced with hydrogens, and on complex **4'**, deduced from **4** by substituting methyl groups to *p*-methoxyphenyls. This study is aimed at understanding the electronic structure and the magnetic properties of tetranuclear chains of nickel atoms, in comparison with previous studies focused on $\text{Ni}_3(\text{dpa})_4\text{Cl}_2$ and $[\text{Ni}_3(\text{dpa})_4]^{x+}$ complexes ($x = 2, 3$).⁹

Computational Method

Calculations and geometry optimizations on **1'**, **2'**, **3'**, [**3'**]⁺, and **4'** have been carried out using the density functional theory (DFT) formalism with the spin unrestricted option, as implemented in the Gaussian03 software,¹⁴ with the B3LYP exchange-correlation functional. All-electron valence double- ζ basis sets (D95V) were used to describe C, O, and H atoms. Full double- ζ (D95) bases were employed and supplemented with one and two d-type polarization functions for N and S, respectively. These polarization functions on S

- (2) (a) Sheu, J.-T.; Lin, C.-C.; Chao, I.; Wang, C.-C.; Peng, S.-M. *Chem. Commun.* **1996**, 315. (b) Kuo, C.-K.; Chang, J.-C.; Yeh, C.-Y.; Lee, G.-H.; Wang, C.-C.; Peng, S.-M. *Dalton Trans.* **2005**, 3696.
- (3) (a) Berry, J. F.; Cotton, F. A.; Murillo, C. A. *Organometallics* **2004**, *23*, 2503. (b) Berry, J. F.; Cotton, F. A.; Murillo, C. A.; Roberts, B. K. *Inorg. Chem.* **2004**, *43*, 2277. (c) Tsao, T.-B.; Lee, G.-H.; Yeh, C.-Y.; Peng, S.-M. *Dalton Trans.* **2003**, 1465. (d) Sheng, T.; Appelt, R.; Comte, V.; Vahrenkamp, H. *Eur. J. Inorg. Chem.* **2003**, 3731. (e) Berry, J. F.; Cotton, F. A.; Murillo, C. A. *Dalton Trans.* **2003**, 3015. (f) Yeh, C.-Y.; Chiang, Y.-L.; Lee, G.-H.; Peng, S.-M. *Inorg. Chem.* **2002**, *41*, 4096. (g) Zhu, L.-G.; Peng, S.-M.; Lee, G. H. *Anal. Sci.* **2002**, *18*, 1067.
- (4) (a) Berry, J. F.; Cotton, F. A.; Daniels, L. M.; Murillo, C. A.; Wang, X. *Inorg. Chem.* **2003**, *42*, 2418. (b) Berry, J. F.; Cotton, F. A.; Lei, P.; Lu, T.; Murillo, C. A. *Inorg. Chem.* **2003**, *42*, 3534. (c) Berry, J. F.; Cotton, F. A.; Lu, T.; Murillo, C. A.; Wang, X. *Inorg. Chem.* **2003**, *42*, 3595. (d) Berry, J. F.; Cotton, F. A.; Lu, T.; Murillo, C. A. *Inorg. Chem.* **2003**, *42*, 4425. (e) Berry, J. F.; Cotton, F. A.; Daniels, L. M.; Murillo, C. A. *J. Am. Chem. Soc.* **2002**, *124*, 3212.
- (5) (a) Shieh, S.-J.; Chao, C.-C.; Lee, G.-H.; Wang, C.-C.; Peng, S.-M. *Angew. Chem., Int. Ed. Engl.* **1997**, *36*, 56. (b) Yeh, C.-Y.; Chou, C.-H.; Pan, K.-C.; Wang, C.-C.; Lee, G.-H.; Su, Y.-O.; Peng, S. M. *J. Chem. Soc., Dalton Trans.* **2002**, 2670.
- (6) Chen, Y.-H.; Lee, C.-C.; Wang, C.-C.; Lee, G.-H.; Lai, S.-Y.; Li, F.-Y.; Mou, C.-Y.; Peng, S.-M. *Chem. Commun.* **1999**, 1667.
- (7) Peng, S.-M.; Wang, C.-C.; Jang, Y.-L.; Chen, Y.-H.; Li, F.-Y.; Mou, C.-Y.; Leung, M.-K. *J. Magn. Magn. Mater.* **2000**, *209*, 80.
- (8) (a) Rohmer, M.-M.; Bénard, M. *J. Am. Chem. Soc.* **1998**, *120*, 9372. (b) Rohmer, M.-M.; Bénard, M.; Malrieu, J.-P. *J. Am. Chem. Soc.* **2001**, *123*, 9126. (c) Benbellat, N.; Rohmer, M.-M.; Bénard, M. *Chem. Commun.* **2001**, 2368.
- (9) Kiehl, P.; Rohmer, M.-M.; Bénard, M. *Inorg. Chem.* **2004**, *43*, 3151.
- (10) Li, F.-Y.; Chen, L.; Mou, C.-Y.; Peng, S.-M.; Wang, Y. *Int. J. Mol. Sci.* **2002**, *3*, 38.
- (11) Kitagawa, Y.; Shoji, M.; Koizumi, K.; Kawakami, T.; Okumura, M.; Yamaguchi, K. *Polyhedron* **2005**, *24*, 2751.
- (12) Cotton, F. A.; Daniels, L. M.; Murillo, C. A.; Wang, X. *Chem. Commun.* **1998**, 39.

- (13) Lai, S.-Y.; Lin, T.-W.; Chen, Y.-H.; Wang, C.-C.; Lee, G.-H.; Yang, M.-h.; Leung, M.-k. Peng, S.-M. *J. Am. Chem. Soc.* **1999**, *121*, 250.
- (14) Frisch, M. J.; Trucks, G. W.; Schlegel, H. B.; Scuseria, G. E.; Robb, M. A.; Cheeseman, J. R.; Montgomery, J. A., Jr.; Vreven, T.; Kudin, K. N.; Burant, J. C.; Millam, J. M.; Iyengar, S. S.; Tomasi, J.; Barone, V.; Mennucci, B.; Cossi, M.; Scalmani, G.; Rega, N.; Petersson, G. A.; Nakatsuji, H.; Hada, M.; Ehara, M.; Toyota, K.; Fukuda, R.; Hasegawa, J.; Ishida, M.; Nakajima, T.; Honda, Y.; Kitao, O.; Nakai, H.; Klene, M.; Li, X.; Knox, J. E.; Hratchian, H. P.; Cross, J. B.; Adamo, C.; Jaramillo, J.; Gomperts, R.; Stratmann, R. E.; Yazyev, O.; Austin, A. J.; Cammi, R.; Pomelli, C.; Ochterski, J. W.; Ayala, P. Y.; Morokuma, K.; Voth, G. A.; Salvador, P.; Dannenberg, J. J.; Zakrzewski, V. G.; Dapprich, S.; Daniels, A. D.; Strain, M. C.; Farkas, O.; Malick, D. K.; Rabuck, A. D.; Raghavachari, K.; Foresman, J. B.; Ortiz, J. V.; Cui, Q.; Baboul, A. G.; Clifford, S.; Cioslowski, J.; Stefanov, B. B.; Liu, G.; Liashenko, A.; Piskorz, P.; Komaromi, I.; Martin, R. L.; Fox, D. J.; Keith, T.; Al-Laham, M. A.; Peng, C. Y.; Nanayakkara, A.; Challacombe, M.; Gill, P. M. W.; Johnson, B.; Chen, W.; Wong, M. W.; Gonzalez, C.; Pople, J. A. *Gaussian 03*, Revision B.05; Gaussian, Inc., Pittsburgh, PA, 2003.

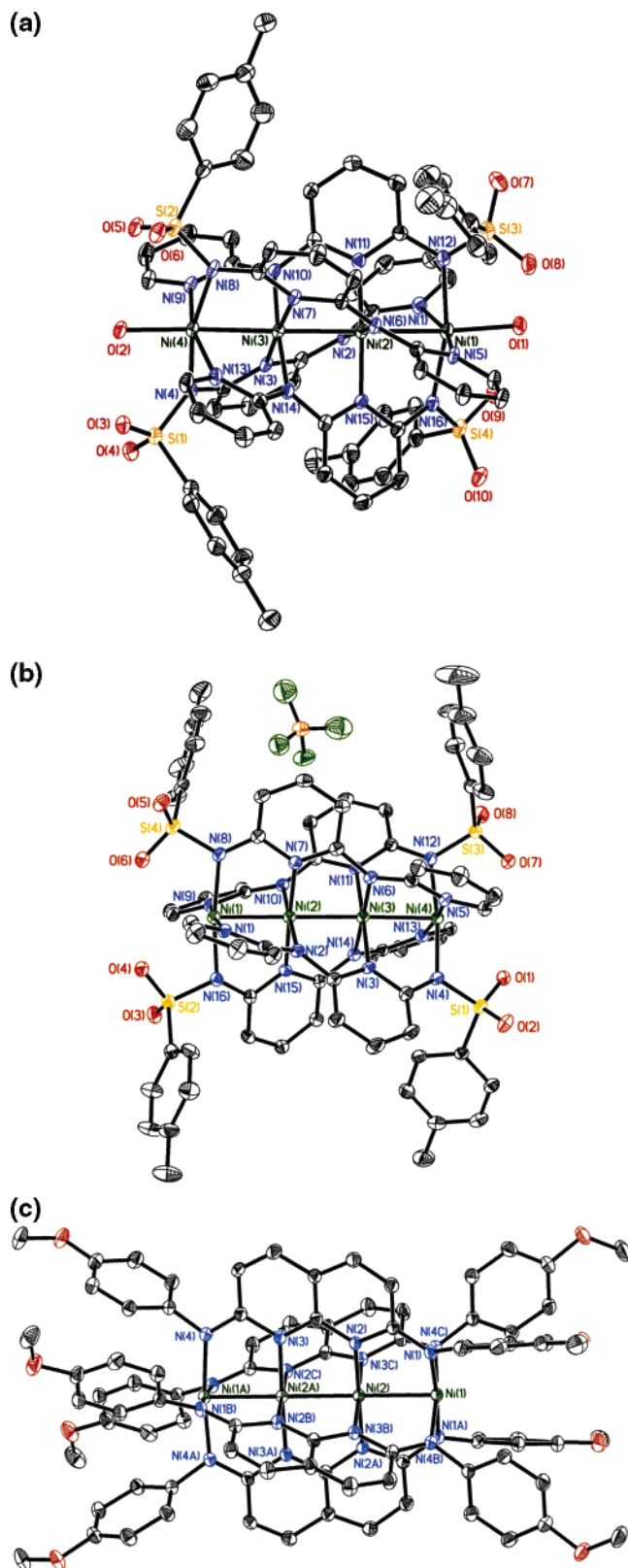


Figure 1. ORTEP view of **2** (top), **[3]⁺** (middle), and **4** (bottom). Thermal ellipsoids are drawn at the 30% probability level. Hydrogen atoms are omitted for clarity.

(exponents 1.064 and 0.266) were found necessary to accurately model the tosylate substituents, and more specifically to reproduce the observed S–N bond length. The valence shell of nickel was described at the double- ξ level

(LanL2DZ basis) and the neon core was modeled with the Los Alamos core potential. The antiferromagnetic low-spin state of **2** has been characterized and its geometry optimized using the broken symmetry (BS) approach first proposed by Ginsberg¹⁵ and then developed and applied by Noodleman¹⁶ and by others.¹⁷ The exchange parameter J_{AB} between two magnetic centers A and B is defined in terms of the Heisenberg–Dirac–van Vleck (HDVV) Hamiltonian:¹⁸

$$\hat{H}^{\text{HDVV}} = -2J_{AB}\hat{S}_A\cdot\hat{S}_B \quad (1)$$

If each magnetic center is assigned a total spin of 1, the eigenfunctions of the HDVV Hamiltonian are the five components of a quintet Q, the three components of a triplet T, and a singlet S. The corresponding eigenvalues are $-2J_{AB}$, $+2J_{AB}$ and $+4J_{AB}$, respectively.¹⁹ Since the energy $^{\text{BS}}E$ of the single-determinant broken-symmetry solution is a weighted average of the energies of the pure spin multiplets,^{16c,19} the energy difference $^{\text{BS}}E - ^{\text{HS}}E$, where $^{\text{HS}}E$ corresponds to the energy of the highest spin state, should be related in a standard ab initio framework to the energy of the true singlet and to the J_{AB} value by means of an appropriate spin projection procedure. Within the DFT framework, the projection approach is controversial. Ruiz et al.²⁰ argue that the unprojected BS state represents the best approximation to the real antiferromagnetic state within the single determinant Kohn–Sham theory. However, we persist in using projected energy values since they provide a lower bound to the true energy²¹ and have the merit of attracting attention to the importance of overlap between magnetic orbitals. We

- (15) Ginsberg, A. P. *J. Am. Chem. Soc.* **1980**, *102*, 111.
 (16) (a) Noodleman, L. *J. Chem. Phys.* **1981**, *74*, 5737. (b) Noodleman, L.; Baerends, E. J. *J. Am. Chem. Soc.* **1984**, *106*, 2316. (c) Noodleman, L.; Davidson, E. R. *J. Chem. Phys.* **1986**, *109*, 131. (d) Noodleman, L.; Norman, J. G., Jr.; Osborne, J. H.; Aizman, A.; Case, D. A. *J. Am. Chem. Soc.* **1985**, *107*, 3418. (f) Noodleman, L.; Case, D. A.; Aizman, A. *J. Am. Chem. Soc.* **1988**, *110*, 1001. (g) Noodleman, L.; Peng, C. Y.; Case, D. A.; Mousesca, J. M. *Coord. Chem. Rev.* **1995**, *144*, 199.
 (17) (a) Caballol, R.; Castell, O.; Illas, F.; Moreira, F. de P. R.; Malrieu, J.-P. *J. Phys. Chem. A* **1997**, *101*, 7860. (b) Martin, R. L.; Illas, F. *Phys. Rev. Lett.* **1997**, *79*, 1539. (c) Illas, F.; Martin, R. L. *J. Chem. Phys.* **1998**, *108*, 2519. (d) Cabrero, J.; Calzado, C. J.; Maynau, D.; Caballol, R.; Malrieu, J.-P. *J. Phys. Chem. A* **2002**, *106*, 8146. (e) Petrie, S.; Stranger, R. *Inorg. Chem.* **2002**, *41*, 2341. (f) Stranger, R.; Petrie, S. *J. Chem. Soc., Dalton Trans.* **2002**, 1163. (g) Petrie, S.; Stranger, R. *Polyhedron* **2002**, *21*, 1163, and references therein. (h) Delfs, C. D.; Stranger, R. *Inorg. Chem.* **2001**, *40*, 3061. (i) Duclausaud, H.; Borshch, S. A. *J. Am. Chem. Soc.* **2001**, *123*, 2825. (j) Blasco, S.; Demachy, I.; Jean, Y.; Lledós, A. *New J. Chem.* **2002**, *26*, 1118. (k) Blasco, S.; Demachy, I.; Jean, Y.; Lledós, A. *Inorg. Chim. Acta* **2000**, *300–302*, 837. (l) Demachy, I.; Lledós, A.; Jean, Y. *Inorg. Chem.* **1999**, *38*, 5443. (m) Demachy, I.; Jean, Y.; Lledós, A. *Chem. Phys. Lett.* **1999**, *303*, 621. (n) Lledós, A.; Jean, Y. *Chem. Phys. Lett.* **1998**, *287*, 243.
 (18) (a) Dirac, P. A. M. *Proc. R. Soc. London, Ser. A* **1926**, *112*, 661; **1929**, *123*, 714. (b) Heisenberg, W. *Z. Phys.* **1926**, *38*, 411. (c) van Vleck, J. H. *Theory of Electric and Magnetic Susceptibilities*; Oxford University Press: London, 1932. (d) Kahn, O. *Molecular Magnetism*; Wiley-VCH: New York, 1993.
 (19) (a) Illas, F.; Moreira, I. de P. R.; de Graaf, C.; Barone, V. *Theor. Chem. Acc.* **2000**, *104*, 265. (b) Adamo, C.; Barone, V.; Mencini, A.; Broer, R.; Filatov, M.; Harrison, N. M.; Illas, F.; Malrieu, J. P.; Moreira, I. de P. R. *J. Chem. Phys.* **2006**, *124*, 107101.
 (20) (a) Ruiz, E.; Alvarez, S.; Cano, J.; Polo, V. *J. Chem. Phys.* **2005**, *123*, 164110. (b) Ruiz, E. *Struct. Bond.* **2004**, *113*, 71. (c) Ruiz, E.; Alvarez, S.; Rodríguez-Fortea, A.; Alemany, P.; Pouillon, Y.; Mas-sobrio, C. In *Magnetism: Molecules to Materials*; Miller, J. S., Drillon, M., Eds.; Wiley-VCH: Weinheim, Germany, 2001; Vol. 2, p 227.

used the approximate projection proposed by Yamaguchi et al, valid for two and three magnetic centers,²² which relies on the dependence of J_{AB} upon the spin contamination of the BS solution:

$$2J_{ab} = 2(\langle^{BS}E - \langle^{HS}E\rangle) / (\langle^{HS}\langle S^2 \rangle - \langle^{BS}\langle S^2 \rangle\rangle) \quad (2)$$

$\langle^{HS}\langle S^2 \rangle$ and $\langle^{BS}\langle S^2 \rangle$ denote the total spin angular momentum calculated in the high spin and in the broken symmetry solutions, respectively. $\langle^{BS}\langle S^2 \rangle$ can in principle vary from the eigenvalue of the real low-spin state to a maximal value $\langle S^2 \rangle_{\max}$, involving the spin eigenvalues of the contaminants. $\langle^{BS}\langle S^2 \rangle = 0$ corresponds to the ideal case of a perfect overlap between the magnetic centers, whereas $\langle^{BS}\langle S^2 \rangle \sim \langle S^2 \rangle_{\max}$ indicates a negligible overlap.²² All geometry optimizations have been carried out by assuming the symmetry constraints of the D_2 , or—for the broken-symmetry calculations—of the C_2 symmetry point groups for $1'$, $2'$, $3'$, and $[3']^+$ and of D_4 and C_4 point groups for $4'$.

MO Analysis of Nickel Polypyridylamide Complexes.

The sequence of 5d metal orbitals expected for EMACs with a number m of metal atoms has been reported and analyzed previously.^{4a,5b,8,9,11} These orbitals are distributed into separate subsets according to their σ , π , or δ character. Note that the combinations of xy and x^2-y^2 atomic orbitals give rise to two separate δ subsets, depending on the orientation of the orbital lobes with respect to the equatorial ligands. On one hand, an orientation bisecting the N–M–N angles generates m low-energy molecular orbitals (MOs) of δ character displaying weak interactions with the π orbitals of the polypyridylamide ligands. On the other hand, a second set of m MOs with higher energy and metal–ligand antibonding character is generated by combining orbitals with lobes collinear with the M–N directions. In either set of δ MOs, the orientation of the metal orbitals follows the helicity of the polypyridylamide ligands, which further reduces the δ interaction between consecutive metal atoms. The magnetic and structural properties of EMACs and, more specifically, of nickel metal chains, therefore, depend on the occupancy of these metal orbital combinations, but can be alternatively analyzed in terms of the ligand field theory. Previous studies, either experimental or theoretical, have shown that the two approaches complement each other.^{4a,9}

Considering $\text{Ni}_3(\text{dpa})_4\text{Cl}_2$, as far as the delocalized interactions along the metal chain can be neglected, the outermost Ni^{II} atoms undergo a square-pyramidal field, favorable to a high-spin ($S = 1$) electronic configuration, whereas the central nickel is expected to be low spin ($S = 0$) regarding

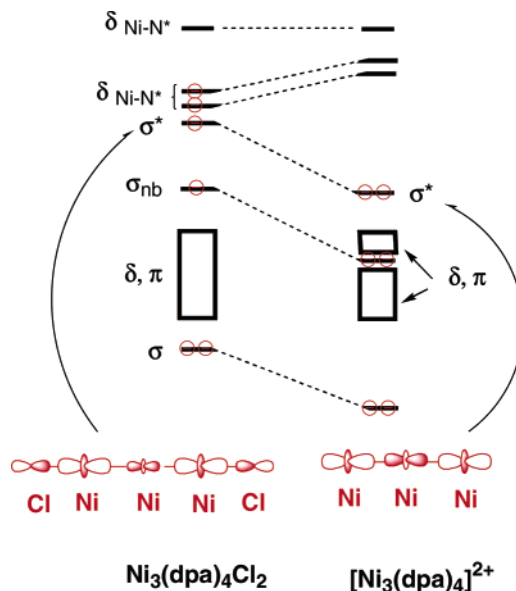


Figure 2. Sequence and occupancy of the metal orbitals in $\text{Ni}_3(\text{dpa})_4\text{Cl}_2$ and in $[\text{Ni}_3(\text{dpa})_4]^{2+}$, a model for the diamagnetic complex $[\text{Ni}_3(\text{BPAP})_4]^{2-}$.

its square planar environment.^{4a,23} The ground state of $\text{Ni}_3(\text{dpa})_4\text{Cl}_2$ can therefore be predicted to exhibit a four-electron antiferromagnetic interaction between the magnetic centers at both ends of the molecule. In terms of symmetry-adapted molecular orbitals, this antiferromagnetic ground state results from the distribution of four metal electrons into a set of four semioccupied MOs, namely, the two highest σ -type combinations with respective nonbonding and antibonding character and the two high-energy δ MOs weighted on the outermost metals and their equatorial environment (Figure 2). Note that the half-occupancy of these δ MOs with metal–ligand antibonding character induces a distinctive stretching of the outermost M–N bond lengths with respect to the central ones ($\Delta d \sim 0.2 \text{ \AA}$).²³ Experiment and calculations agree on these conclusions.^{4a,9} In return, the half-occupancy of the σ^* MO, opposed to the full occupancy of the bonding σ combination, provides the metal chain with a weak, but real, delocalized interaction.⁹ The magnetic and structural characterization of a series of $\text{Ni}_{2n+3}(n\text{-ppa})_4\text{Cl}_2$ metal chains with 3, 5, 7, and 9 metal atoms confirms that the strong σ -donor character of the chlorine axial ligands raises the electronic state of the outermost metal atoms into high spin, elongates by $\sim 0.2 \text{ \AA}$ the $\text{Ni}_{\text{outer}}\text{-N}$ bond lengths, and yields an antiferromagnetic ground state for all four nickel chain complexes.⁷

The dianion of 2,6[bis(phenylamino)]pyridine, BPAP^{2-} , was found to stabilize trimetallic chains of metal atoms, but the presence of bulky phenyl substituents impedes the approach of axial ligands.²⁴ The dianion $[\text{Ni}_3(\text{BPAP})_4]^{2-}$ is therefore isoelectronic with $\text{Ni}_3(\text{dpa})_4\text{Cl}_2$, but all three metal atoms are now in a square planar ligand environment and expected to be low-spin. In agreement with the rules of ligand field theory, the complex was indeed found to be diamag-

- (21) (a) Wittbrodt, J. M.; Schlegel, H. B. *J. Chem. Phys.* **1996**, *105*, 6574. (b) Goldstein, E.; Beno, B.; Houk, K. N. *J. Am. Chem. Soc.* **1996**, *118*, 6036. (c) Rodriguez, J. H.; Wheeler, D. E.; McCusker, J. K. *J. Am. Chem. Soc.* **1998**, *120*, 12051.
- (22) (a) Yamaguchi, K.; Fukui, H.; Fueno, T. *Chem. Lett.* **1986**, 625. (b) Mitani, M.; Mori, H.; Takano, Y.; Yamaki, D.; Yoshioka, Y.; Yamaguchi, K. *J. Chem. Phys.* **2000**, *113*, 4035. (c) Onishi, T.; Soda, T.; Kitagawa, Y.; Takano, Y.; Daisuke, Y.; Takamizawa, S.; Yoshioka, Y.; Yamaguchi, K. *Mol. Cryst. Liq. Cryst.* **2000**, *143*, 133. (d) Onishi, T.; Takano, Y.; Kitagawa, Y.; Kawakami, T.; Yoshioka, Y.; Yamaguchi, K. *Polyhedron* **2001**, *20*, 1177. (e) For a recent review and extension, see: Yamanaka, S.; Takeda, R.; Shoji, M.; Kitagawa, Y.; Honda, H.; Yamaguchi, K. *Int. J. Quantum Chem.* **2005**, *105*, 605.

- (23) Clérac, R.; Cotton, F. A.; Dunbar, K. R.; Murillo, C. A.; Pascual, I.; Wang, X. *Inorg. Chem.* **1999**, *38*, 2655.
- (24) Cotton, F. A.; Daniels, L. M.; Lei, P.; Murillo, C. A.; Wang, X. *Inorg. Chem.* **2001**, *40*, 2778.

Table 1. Crystal Data for Compounds **2**, **[3]⁺**, and **4**

	2 ·2H ₂ O·ClCH ₂ CH ₂ Cl	[3] (BF ₄)·5ClCH ₂ CH ₂ Cl	4 ·9CH ₂ Cl ₂
formula	C ₇₀ H ₆₄ Cl ₂ N ₁₆ O ₁₀ S ₄ Ni ₄	C ₇₈ H ₇₆ BF ₄ Cl ₁₀ F ₄ N ₁₆ O ₈ S ₄ Ni ₄	C ₉₇ H ₉₀ Cl ₁₈ N ₁₆ Ni ₄ O ₈
formula weight	1723.35	2169.94	2480.79
temperature (K)	150(2)	150(1)	150(1)
diffractometer	NONIUS, Kappa CCD	NONIUS, Kappa CCD	NONIUS, Kappa CCD
wavelength (Å)	0.710 73	0.710 73	0.710 73
crystal system	monoclinic	monoclinic	orthorhombic
space group	<i>P</i> 2 ₁ / <i>c</i>	<i>P</i> 2 ₁ / <i>n</i>	Fddd
<i>a</i> (Å)	13.3384(2)	17.7808(5)	21.5219(3)
<i>b</i> (Å)	21.1767(4)	14.4123(4)	28.3611(5)
<i>c</i> (Å)	25.5458(4)	35.9154(10)	33.4189(6)
α (deg)	90	90	90
β (deg)	90.2406(9)	101.0758(6)	90
γ (deg)	90	90	90
<i>V</i> (Å ³)/ <i>Z</i>	7141.2(2)/4	9032.3(4)/4	20398.4(6)/8
absorption coefficient (mm ⁻¹)	1.603	1.596	1.264
crystal size (mm)	0.20 × 0.15 × 0.03	0.45 × 0.20 × 0.08	0.20 × 0.15 × 0.15
θ range for data collection (deg)	1.54–25.00	1.16–25.00	1.88–27.50
reflection collected	44 704	75 328	44 640
independent reflections	12478 (<i>R</i> _{int} = 0.0655)	15860 (<i>R</i> _{int} = 0.0681)	5856 (<i>R</i> _{int} = 0.0498)
<i>R</i> _F , <i>R</i> _{wF} ² (all data) ^a	0.1008, 0.1707	0.1038, 0.2243	0.0828, 0.1771
<i>R</i> _F , <i>R</i> _{wF} ² (<i>I</i> > 2σ(<i>I</i>)) ^a	0.0559, 0.1464	0.0759, 0.2073	0.0555, 0.1583
GOF	1.009	1.094	1.084

$$^a R_F = \sum |F_o - F_c| / \sum |F_o|; R_{wF}^2 = [\sum w|F_o^2 - F_c^2|^2 / \sum wF_o^4]^{1/2}.$$

netic, and the outermost Ni–N distances were observed in the same range as the central ones.²⁴ A calculation carried out on the model system [Ni₃(dpa)₄]²⁺ reached similar conclusions.⁹ In the language of molecular orbitals, the removal of the axial ligands resulted in a stabilization of all three combinations of d_{z²} orbitals, due to the vanishing of the antibonding Ni_{outer}–Cl interactions along the *z* axis (Figure 2). More specifically, an energy gap favorable to a diamagnetic ground state was created by the stabilization of the σ* MO with respect to the set of high-lying δ orbitals. This HOMO–LUMO gap is further enhanced by an uprise of the δ levels induced by the contraction of the Ni_{outer}–N distances (Figure 2).

Finally, the oxidation of Ni₃(dpa)₄Cl₂ resulted in the removal of the axial chlorines, replaced by three tetrafluoroborate counterions without significant contact with the metal chain. The disappearance of axial coordination yielded a dramatic contraction of the coordination sphere of the outermost metals, including a 0.17 Å contraction of the metal–metal distance, and a change of the magnetic status of the molecule from antiferromagnetic to paramagnetic.^{4a,c,e} These drastic changes were also interpreted in terms of the collapse of the σ MOs induced by the change of the coordination environment from square pyramidal to nearly square planar.⁹

Structure. Experimental Structures of **2**, **[3]⁺**, and **4**.

A general method for the synthesis of a series of oligo-α-pyridylamido ligands has been developed.²⁵ The desired ligand, H₂Tsdpda, can be prepared from the reaction of dipyridyldiamine (H₃dpda) with 1.2 equiv of *p*-toluenesulfonyl chloride (*p*-TsCl) in pyridine. The brown solution, on being stirred for 1 h, turned red-brown. It was then added

dropwise to aqueous HCl (15% aq). The yellow precipitate was filtered off, washing with acetone, and recrystallized from DMF. The ligand H₂DAniDANy was synthesized from the similar procedure²⁵ of H₂bpyany in 33% yield by the palladium-catalyzed cross-coupling reaction of 2,7-dichloro-1,8-naphthyridine with *p*-anisidine in the presence of *t*-BuONa. Compounds [Ni₄(μ₄-Tsdpda)₄(H₂O)₂] (**2**) and [Ni₄(μ₄-DAniDANy)₄] (**4**) can be synthesized by the reaction of Ni(OAc)₂·4H₂O with the corresponding ligand using naphthalene as the solvent. The one-electron oxidized product [Ni₄(μ₄-Tsdpda)₄](BF₄) (**[3]⁺**) was obtained by reacting the neutral complex with silver tetrafluoroborate. Summaries of the crystal data for compounds **2**, **[3]⁺**, and **4** are given in Table 1.

For compound **2**, the structure consists of a linear chain of four nickel atoms bridged by four Tsdpda²⁻ ligands in a (2,2)-trans fashion. The molecular structure of **2** is shown in Figure 1. The internal Ni–Ni bond length is 2.32 Å and Ni–N distances fall into the range 1.87–1.92 Å, whereas the external Ni–Ni bond lengths are about 2.38 Å and Ni–N distances lie in the range 2.07–2.10 Å. Neglecting the Ni–Ni interactions, the inner nickel ions have square planar geometry and are in low-spin states, whereas the outer nickel ions have square pyramidal geometry and are in high-spin states. The structure of the one-electron-oxidized compound **[3]⁺** basically remains, but the axial water molecules have been removed. Each of the four nickel(II) ions are coordinated by four nitrogen atoms with a square-planar arrangement. All the Ni–N distances lie in the range 1.89–1.95 Å, which indicates that the nickel ions are in low-spin states. In comparison with **2** and **[3]⁺**, the Ni–Ni bond distances of 2.312, 2.316, and 2.261 Å in compound **[3]⁺** are shorter than in those of **2** (2.385, 2.386, and 2.32 Å) (Table 2). The metal–metal bond formation in **[3]⁺** is attributed to these shortenings.

The structure of compound **4** also consists of a linear chain of nickel atoms bridged by four DAniDANy²⁻. A slight

(25) (a) Hasanov, H.; Tan, U.-K.; Wang, R.-R.; Lee, G.-H.; Peng, S.-M. *Tetrahedron Lett.* **2004**, *45*, 7765. (b) Chien, C.-H.; Chang, J.-C.; Yeh, C.-Y.; Lee, G.-H.; Fang, J.-M.; Peng S.-M. *Dalton Trans.* **2006**, 2106. (c) Chien, C.-H.; Chang, J.-C.; Yeh, C.-Y.; Lee, G.-H.; Fang, J.-M.; Peng S.-M. *Dalton Trans.* **2006**, 3249.

Table 2. Selected Interatomic Distances (Å), Angles, and H₂O/H₂O Torsional Angle (deg) Observed for **2**, [**3**]⁺, **1**, and **4** and Computed for Their Models^a

	2' :		3'		[3'] ⁺		1'		1: obs ^b	4'		4: obs ^b
	comp, BS ^c	2: obs ^b	comp, high spin	comp, low spin	comp, low spin	obs ^b	comp, high spin	comp, low spin		comp, high spin	comp, low spin	
Ni1–Ni2 ^c	2.406	2.385	2.387	2.365	2.344	2.309	2.354	2.364	2.328	2.359	2.372	2.356
Ni2–Ni3	2.359	2.321	2.366	2.331	2.301	2.253	2.238	2.322	2.301	2.264	2.357	2.323
Ni1–O	2.002	2.042										
Ni1–N _{pyridine}	2.117	2.086	2.081	1.944	1.936	1.921	1.968	1.966	1.938			
Ni1–N _{amido}	2.149	2.096	2.079	1.961	1.949	1.925	1.902	1.894	1.913	1.936	1.918	1.912
Ni2–N _{pyridine}	1.968	1.922	1.977	1.967	1.955	1.917	2.066	1.935	1.916	2.074	1.950	1.912
Ni2–N _{amido}	1.900	1.875	1.906	1.910	1.901	1.875	2.075	1.935	1.911			
S–O3	1.467	1.440	1.465	1.465	1.460							
S–O4	1.479	1.448	1.479	1.468	1.467							
S–N	1.609	1.599	1.600	1.622	1.631							
Ni _{outer} ···O _{tosyl}			2.625	2.84	2.762	2.76						
H ₂ O···O _{tosyl}	1.96											
N _{amido} –Ni1–N _{amido}	166.2	165.6	166.0	173.0	172.7	171.7						
N _{pyridine} –Ni1–N _{pyridine}	163.8	163.5	169.4	173.7	174.4	173.3						
N _{amido} –Ni2–N _{amido}	175.0	175.4	177.4	179.2	179.3	178.3						
N _{pyridine} –Ni2–N _{pyridine}	176.6	176.9	175.1	177.9	177.9	177.0						
N _{pyridine} –Ni1–N _{amido}								173.9	174.0			
N _{pyridine} –Ni2–N _{amido}								179.1	177.8			
θ ^e	34	52										

^a Antiferromagnetic ground state, approximated by the broken symmetry solution, for **2'**, diamagnetic ground state for **3'**, and paramagnetic ground state (doublet) for [**3'**]⁺. ^b Averaged. ^c Broken-symmetry solution. The geometry for the high-spin state is nearly identical. ^d Ni1, Ni4 ≡ Ni_{outer}; Ni2, Ni3 ≡ Ni_{inner}. ^e H₂O/H₂O angle

difference is that all nickel ions are in square planar fashion and low-spin states, which results in $S = 0$ for the whole complex. The bond lengths for internal and terminal Ni–Ni are 2.323 and 2.356 Å respectively. The Ni–N distances are around 1.912 Å, which corresponds to a typical bond length of square planar diamagnetic nickel complex.

Computed Structures of **2', **3'**, and [**3'**]⁺.** Geometry optimizations have been carried out on the antiferromagnetic ground state of **2'**, on the high-spin ($S = 2$) and low-spin ($S = 0$, diamagnetic singlet) states of **3'**, and on the low-spin state of [**3'**]⁺ ($S = 1/2$; paramagnetic). The geometry of the BS solution describing the antiferromagnetic state and that of the associated high-spin state are nearly identical. Selected information on the observed and computed structures is displayed in Table 2.

The BS solution reproduces quite nicely most structural features of **2** (Table 2). All computed distances deviate from the averaged observed values by less than 0.05 Å. The Ni_{inner}–N bond lengths, either observed or computed, consistently reflect the relative basicities of the surrounding ligands: the protonated amido ends are closer to the metal than the pyridine ends ($\Delta d = 0.05$ – 0.07 Å). Surprisingly, the Ni–N distances at the outer metal atoms display the reverse order, but no direct comparison with the inner distances can be made from **2** and **2'** due to the relative expansion of the equatorial environment of Ni_{outer}, similar to that observed for Ni_{2n+3}(*n*-ppa)₄Cl₂ metal chains (Table 2).

Two electronic configurations have been considered for complex **3'**, deduced from **2'** by the removal of axial ligands. The geometry obtained for the high-spin ($S = 2$) configuration differs from that of **2'** by a contraction of the Ni_{outer}–N distances, especially on the toluenesulfonylamido ends (0.07 Å). All other distances remain similar. In the low-spin ground states of complexes **3'** and [**3'**]⁺, stripped from axial ligands,

the Ni–N distances around both metal sites become directly comparable and it clearly appears that the presence of the sulfonyl substituents weakens the proximate Ni–N bonds, resulting in a computed bond stretching of ~ 0.05 Å with respect to the Ni_{inner}–N_{amido} distance. The outermost Ni–N_{sulfonylamido} distances in **3'** are therefore computed to be slightly larger than the Ni–N_{pyridine} ones, despite the protonation at the amido end. A similar elongation, from 1.875 to 1.925 Å, is observed in [**3'**]⁺, and the average values for both types of Ni_{outer}–N distances are nearly equal (Table 2).

The metal–metal bond lengths observed for **2** are very close to those characterized for Ni₅(tpda)₄Cl₂. More generally, the following trends observed for the [Ni₅]^{10/11+} chains with respect to their trinuclear counterparts are reproduced in **2** and [**3'**]⁺:

(i) Both types of Ni–Ni bonds in **2** are shorter than the distances of 2.42–2.44 Å observed for Ni₃(dpa)₄Cl₂, and the inner bonds are shorter than the outer ones.

(ii) Oxidation, together with the removal of the axial ligands, contracts all Ni–Ni bonds by 0.07–0.09 Å. This contraction accounts for the change of the coordination environment of Ni_{outer} from square pyramidal to square planar, better illustrated by the opening of the N–Ni_{outer}–N angles from $\sim 165^\circ$ to $\sim 173^\circ$ (Table 2). However, the removal of axial ligands is not sufficient to promote a real square planar coordination if it does not entail a transition from high spin to low spin in the metal electronic state. The computed structure of the water-free complex **3'** in the high-spin state shows that the terminal Ni atoms still protrude out of the equatorial plane with N–Ni_{outer}–N angles below 170° . A transition to low-spin state opens these angles by 4.3° and 7.0° (Table 2).

The computed Ni–Ni distances agree well with the X-ray data, accounting for a systematic stretching of ~ 0.03 Å. Note

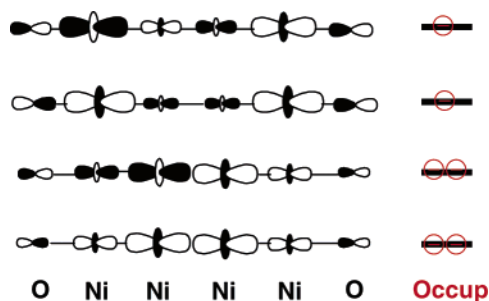


Figure 3. The symmetry-adapted σ -type MOs of $2'$ and their occupancies. Magnetic orbitals are singly occupied.

that the Ni–Ni distances computed for the diamagnetic state of $3'$ are intermediate between those obtained for $2'$ and $[3']^+$ (Table 2). The evolution of the Ni–Ni bond lengths from $2'$ to $3'$ (low-spin) and to $[3']^+$ results from the intricate combination of two factors: (i) the tendency of the outermost Ni–Ni distances to contract when a square planar coordination is favored ($3'$ in low-spin state, $[3']^+$) and (ii) the single or double occupancy of the two σ -type orbitals highest in energy, displaying antibonding character with respect to two or to all three Ni–Ni contacts (Figure 3). Single occupancy for both MOs is achieved for $2'$ and for the high-spin state of $3'$, whereas the highest MO only is singly occupied for $[3']^+$. Both orbitals are doubly occupied in the low-spin state of $3'$, but the lack of any delocalized σ bonding is overcompensated by the move toward a square planar coordination of Ni_{outer} .

An evidential discrepancy between the structure observed for 2 and that computed for $2'$ concerns the angle θ between the planes of the two water ligands. This angle is widely open (52°) in the real complex and closer to planarity (34°) in the model. Both water molecules are involved in intramolecular hydrogen bonds with the sulfonyl groups and the orientation of these bonds is indeed affected by the presence of the phenyl substituents. It has been verified, however, by constraining θ to 90° in subsequent calculations that the relative orientation of the water molecules has no significant influence on the magnetic coupling.

Electronic Ground States for $2'$, $3'$, and $[3']^+$. As for the $Ni_{2n+3}(n\text{-ppa})_4Cl_2$ metal chains with odd number of Ni atoms, the electronic ground state of $2'$ results from the magnetic coupling between four metal electrons originating in the high-spin d^8 metal atoms located at both ends of the chain. In terms of symmetry-adapted molecular orbitals, these electrons are accommodated (i) on two δ -type spin orbitals with $Ni_{\text{outer}}\text{-N}$ antibonding character and (ii) on the two σ -type combinations highest in energy, displaying a major weight on the outermost Ni atoms, though delocalized over the whole metal chain (Figures 3 and 4).

After complete geometry optimization in both spin states, the high spin state ($S = 2$) and the associated antiferromagnetic singlet of complex $3'$ were computed to be more stable than the diamagnetic state by $6.0 \text{ kcal mol}^{-1}$. Although the neutral, dehydrated complex has not been characterized yet, this result appears surprising for various reasons: (i) the complexes exhibiting a linear framework of Ni^{II} atoms and devoid of axial ligands characterized to date, such as

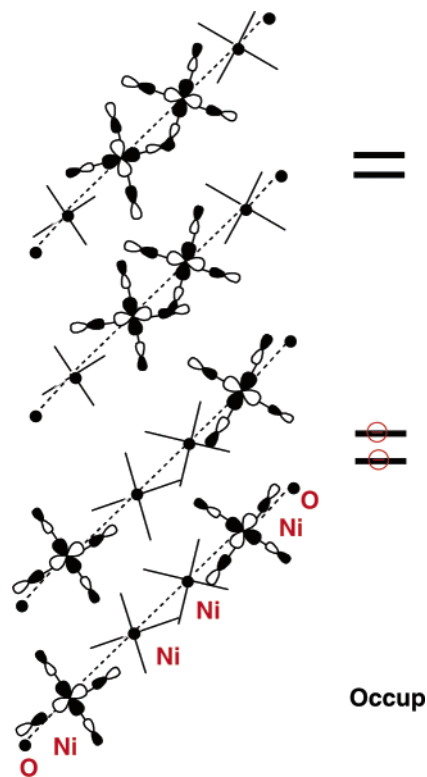


Figure 4. The symmetry-adapted δ -type MOs of $2'$ and their occupancies. Magnetic orbitals are singly occupied.

$[Ni_3(\text{BPAP})_4]^{2-}$ or $Ni_4(\text{phdpda})_4$, were observed to be diamagnetic;^{12,24} (ii) the complex derived from 3 by means of a single-electron oxidation is found to be low-spin ($S = 1/2$); and (iii) calculations carried out on the hypothetical complex $[Ni_3(\text{dpa})_4]^{2+}$ concluded to a diamagnetic ground state in relation with the change of the coordination environment of the terminal nickels from square pyramidal to square planar. A collection of experimental and theoretical results therefore suggests that the removal of axial ligands is sufficient to promote a low-spin configuration for the terminal metals and for the whole complex. It is well established that the high-spin/low-spin energy difference can be influenced by the amount of Hartree–Fock exchange introduced in the hybrid functional, as recently shown by Lawson Daku et al.²⁶ The trends obtained from the comparison of $2'$ and $3'$ with the standard B3LYP functional, however, clearly show a change in the magnetic issues, even though the computed energy gaps could be further optimized within the DFT formalism. A possible explanation involves the sulfonyl groups that are in position to substitute at least partly for the missing axial ligands by means of weak $O\cdots Ni_{\text{outer}}$ interactions. The $O\cdots Ni$ distance of $3'$ was computed to be tight (2.625 \AA) in the high-spin electronic configuration and loose (2.84 \AA) in the diamagnetic state, for which the axial coordination is of no help. However, a reoptimization of the high-spin state with the constraint of keeping $O\cdots Ni$ distances as long as in the diamagnetic state (2.84 \AA) was inconclusive: the energy loss associated with

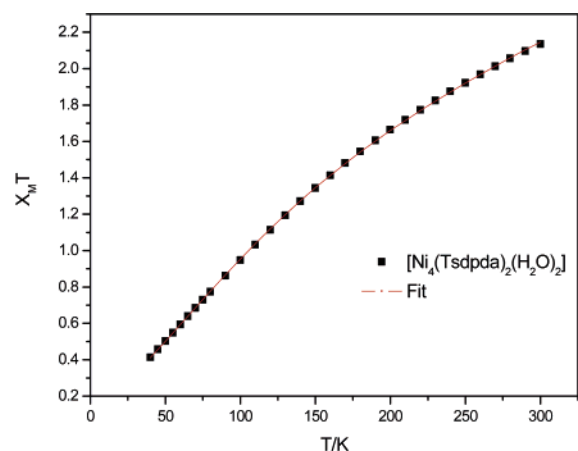
(26) Lawson Daku, L. M.; Vargas, A.; Hauser, A.; Fouqueau, A.; Casida, M. E. *ChemPhysChem* **2006**, *6*, 1393.

this constraint was no more than $2.2 \text{ kcal mol}^{-1}$, not sufficient to reverse the relative stabilities of the two states.

The preference of **3'** for a high-spin or antiferromagnetic ground state might explain why $\text{Ni}_4(\mu_4\text{-Tsdpda})_4$ (**3**) could not be characterized to date without water molecules in the axial position. Chains of nickel atoms indeed remain unsaturated with respect to σ donation as long as the highest delocalized metal MOs with σ character are kept unoccupied or partly occupied. In such a case, axial coordination cannot be avoided, except in the case of a strict steric hindrance.

To get deeper insight into this problem, geometry optimizations have been carried out on two $(\text{Ni}_4)^{8+}$ linear chains that were shown to be diamagnetic and free of axial ligands. $[\text{Ni}_4(\mu_4\text{-phdpda})_4]$ (**1**) was characterized in 1999,¹³ and the short Ni–N distances, all between 1.91 and 1.94 Å (Table 1), found were consistent with the diamagnetic behavior. In the present work, the $[\text{Ni}_4(\mu_4\text{-DAniDANy})_4]$ complex (**4**, DAniDANy = *N,N*-di-*p*-anisyl-2,7-diamino-1,8-naphthyridine) is reported to have similar magnetic and structural character (Table 2). Model complexes **1'** and **4'** were calculated in their lowest singlet and quintet states. In either case, the diamagnetic singlet state was found to be lowest, by 15.7 and 9.0 kcal mol^{-1} , respectively. In both cases, however, the calculated high-spin configuration exhibits a striking difference with the quintets obtained for **3'**, and, previously, with the trinuclear complexes of dipyriddyamide: the high-spin nickel atoms are now located *inside* the metal chain. Consequently, the “long” Ni–N bonds (2.07 Å) are localized on the inner Ni atoms and these metal atoms are pyramidalized due to a severe contraction of the central Ni–Ni distance (2.24–2.26 Å compared to 2.32–2.36 Å in the diamagnetic singlet state; Table 2). Note, however, that for **1'** as for **4'**, the lowest quintet state that was characterized is not equivalent to the precursor of the antiferromagnetic singlet ground state of **2'**, since only three semioccupied molecular orbitals out of four—two δ -type and one σ -type SOMOs—could be localized on the metal framework. The last SOMO appears as an orbital with major ligand character. Various attempts to reintroduce a second σ -type SOMO were unsuccessful, which means that the anticipated state with four metallic SOMOs is an *excited* quintet for **1'** and **4'**, not accessible to DFT calculations. We assign this unexpected behavior to the even distribution of the most basic amido nitrogens among the metal atoms of **1**, which makes more difficult the specific activation of the terminal Ni–N bonds. For $[\text{Ni}_4(\mu_4\text{-DAniDANy})_4]$, the situation is even totally reversed with respect to polypyridylamide complexes, since *all four* deprotonated amino groups are facing the terminal nickel atoms, which destabilizes the corresponding δ metal orbitals with antibonding Ni–N character.

The case of **3**, which also exhibits an even distribution of amido nitrogens, but nevertheless retains high-spin terminal nickels in the absence of axial ligands, therefore seems like an exception in the growing family of $(\text{Ni}_4)^{8+}$ linear chains, very probably related to the presence of two tosylate substituents on the outermost equatorial ligands. These electron-attractor substituents are expected to reduce the



$$H = -2JS, S_z \quad (S_1 = S_2 = 1)$$

$$T = 40\text{--}300 \text{ (K)}$$

P	n	θ	J	g
0.216	2.789e-3	-14.548	-40.304	2

Figure 5. Magnetic behavior of compound **2**: $\chi_M T$ vs T . The solid line is the least-squares fit, and important parameters are given in the inset.

basicity of the deprotonated amino groups and therefore to facilitate the promotion to high spin of the terminal Ni atoms.

The relatively close energetic competition between the diamagnetic state and the high-spin state revealed by the calculations in $(\text{Ni}_4)^{8+}$ free of axial ligands makes possible and highly promising the synthesis and the characterization of related complexes exhibiting fluctuations between diamagnetic and antiferromagnetic ground states. An important character of such bistable complexes could be the property to reversibly bind weakly coordinated axial ligands. Considering the hypothetical dehydration of **2'** leading to **3'**, the energy cost computed in the gas phase for the loss of the two water molecules amounts to 42.6 kcal mol^{-1} . Therefore, the bond energy per ligand is not exceedingly high and the cost of removing the two water molecules from the complex should be compensated at least partly by connecting them to the network of hydrogen bonds characteristic of aqueous medium.

Magnetic Measurements and Calculations. Without axial ligands, complex **4** was thought to be diamagnetic. The $\chi_M T$ values of $\sim 0.098 \text{ emu K mol}^{-1}$ between 300 and 5 K is in agreement with the expected values of 0 emu K mol^{-1} for nickel ions with $S = 0$. Complex **2** with impurity was initially found to be ferromagnetic, and this magnetic behavior, never observed yet in linear metal chains, motivated the theoretical study. However, calculations persistently found the model system **2'** to be antiferromagnetic, with an exchange parameter $-2J$ equal to 35 cm^{-1} with the optimized geometry and to 36 cm^{-1} when the two water molecules are constrained to be perpendicular. A reinvestigation of the magnetic susceptibility on pure crystalline sample eventually confirmed the antiferromagnetic character of **2**. The curve of the temperature-dependent magnetic susceptibility between 40 and 300 K is displayed in Figure 5. The measured data can be fit with good precision (correlation coefficient of 0.9996) by the following equation, a function of $x = 2J_{14}/kT$ in which J_{14} is defined according to eq 1:

$$\chi_M = (1 - P)C' (2e^{2x} + 10e^{6x}) / (1 + 3e^{2x} + 5e^{6x}) + P(2Ng^2\beta^2/3kT) + N\alpha \quad (3)$$

where $C' = Ng^2\beta^2/k(T - \Theta)$, $x = 2J_{14}/KT$, $N = 6.022 \times 10^{23}$, g is the g factor, β is the Bohr magneton, k is Boltzmann's constant ($0.695 \text{ cm}^{-1} \text{ K}^{-1}$), T is the absolute temperature (K), J_{14} is the coupling constant between Ni(1) and Ni(4), Θ is the Weiss temperature (or Weiss constant), $N\alpha$ is the temperature-independent paramagnetism (TIP), and P is the relative content for paramagnetic impurity where spin state $S = 1$ is assumed.

Values taken for eq 3 are shown in the inset of Figure 5. This leads to a value of 80 cm^{-1} for $-2J$. This value completes a series of magnetic measurements carried out on linear chains of three, four, six, seven, and nine Ni(II) atoms and takes an appropriate position on a least-squares fit correlating $-J$ with r^{-3} , r being the distance between the magnetic centers, at both ends of the metal string (Figure 6).

Even though the DFT/B3LYP calculations rightly predicted the antiferromagnetic behavior, the value computed for $-2J$ in $2'$ is underestimated by a factor of ~ 2 (35 cm^{-1} , Table 3). A similar underestimation had been obtained for $\text{Ni}_3(\text{dpa})_4\text{Cl}_2$. This behavior is rather unusual with the B3LYP functional, which generally tends to *overestimate* the strength of the antiferromagnetic couplings, especially when the spin contamination is removed by means of projection techniques.^{17,20} Note, however, that the single point calculations carried out by Kitagawa et al. on $\text{Ni}_5(\text{tpda})_4\text{Cl}_2$ and $\text{Ni}_7(\text{tepra})_4\text{Cl}_2$ also using the B3LYP functional and the same projection formalism do yield the more commonly found overestimation of $-2J$.¹¹ Kitagawa et al., however, concluded that the antiferromagnetic coupling in long Ni chains mainly derives from interactions through bridge ligands and could differ in that respect from the case of shorter chains, in which direct exchange along the metal atoms might provide a significant contribution. It is unfortunately not possible to estimate within the present framework the relative importance of both contributions.²⁷ Calculations on $\text{Ni}_5(\text{tpda})_4\text{Cl}_2$ and other pentanickel chains are in progress to analyze the respective influence of the chain length and of calculation parameters—geometry optimization, Gaussian basis sets, core potentials vs all electron calculations, SCF convergence criteria—on the computation of the small J values associated with these higher nuclearity complexes.

Calculated values of the atomic spin populations are displayed in Table 3. For $2'$ as for the high spin state of $3'$, most of the spin population is concentrated on the external nickel atoms, with minor contributions from all surrounding atoms, including the central nickels. For the doublet ground state of $[3']^+$, however, the spin population becomes more important on the central nickels, which signals an important

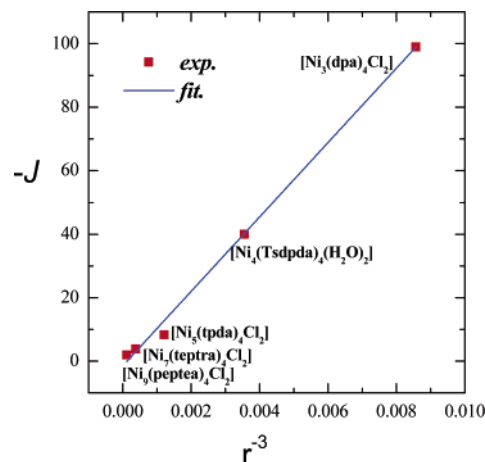


Figure 6. Least-squares fit correlating the magnetic coupling coefficient $-J$ of various linear chains of Ni(II) atoms with the inverse cube of the distance between the magnetic centers.

Table 3. Atomic Spin Populations ($\alpha-\beta$; Electrons) and $\langle S^2 \rangle$ Values Computed for $2'$, $3'$ (high-spin), and $[3']^+$; High-Spin (HS)—Broken-Symmetry (BS) Energy Difference ΔE (cm^{-1}); and Exchange Parameter $-2J$ (cm^{-1}) Computed for $2'$

	$2'$		$3'$:	$[3']^+$:
	HS	BS	HS	doublet
$\alpha-\beta$				
Ni _{outer}	1.64	± 1.65	1.61	0.14
Ni _{inner}	0.06	± 0.06	0.10	0.36
O _{water}	0.049	± 0.045		
N _{outer}	0.054	± 0.054	0.063	
N _{inner}	0.003	± 0.001	0.003	
$\langle S^2 \rangle$	6.017	± 2.011	6.029	
ΔE		70.1		
$-2J$		35.0		

reorganization of the all-antibonding σ^* MO (Table 3). In the quintet state calculated for $1'$ and $4'$, the calculated spin population has been shifted to the *central* nickel atoms, to their equatorial environment, but also delocalized toward the ligands, due to the unanticipated intrusion of a molecular orbital with pure ligand, nonbonding π character into the set of SOMOs of the lowest quintet state.

Experimental Section

Preparation of $[\text{Ni}_4(\mu_4\text{-Tsdpda})_4(\text{H}_2\text{O})_2]$ (2). H_2Tsdpda (0.34 g, 1.00 mmol), $\text{Ni}(\text{OAc})_2 \cdot 4\text{H}_2\text{O}$ (0.7 g, 2.8 mmol), and naphthalene (20 g) were placed in an Erlenmeyer flask. The resulting solution was then stirred at $220 \text{ }^\circ\text{C}$ for 10 h. After cooling the mixture to $80 \text{ }^\circ\text{C}$, hexane (100 mL) was added and the resulting precipitate was filtered out. The solid was extracted with CH_2Cl_2 . The dark purple crystals were obtained by crystallization via slow liquid diffusion of pentane liquid into the 1,2-dichloroethane solution. Yield: 0.16 g (10%). IR (KBr) ν/cm^{-1} : 1136, 1088(S=O), 1601, 1554, 1470 (py). UV/vis (CH_2Cl_2) $\lambda_{\text{max}}/\text{nm}$ ($\epsilon/\text{dm}^3 \text{ mol}^{-1} \text{ cm}^{-1}$): 350 (8.24×10^4), 500 (3.47×10^3). MS(FAB) m/z : 1587 ($[\text{Ni}_4(\mu_4\text{-Tsdpda})_4]^+$). Anal. Calcd for $\text{C}_{72}\text{H}_{68}\text{Cl}_4\text{N}_{16}\text{O}_{10}\text{S}_4$: C, 47.46; H, 3.76; N, 12.30. Found: C, 47.65; H, 4.11; N, 12.21.

Preparation of $[\text{Ni}_4(\mu_4\text{-Tsdpda})_4](\text{BF}_4)$ ($[3']^+$). AgBF_4 (40 mg, 0.2 mol) in CH_3OH (1 mL) was added to a solution of $[\text{Ni}_4(\mu_4\text{-Tsdpda})_4(\text{H}_2\text{O})_2]$ (160 mg, 0.1 mol) in CH_2Cl_2 (50 mL). The resulting mixture was stirred for 1 h and the precipitate was filtered out. The solvent was removed under pressure. Crystals were obtained by crystallization via slow diffusion of pentane vapor into

(27) The superexchange character of the antiferromagnetic coupling involving high-energy δ orbitals as magnetic orbitals in polypyridylamide complexes has been evidenced in the case of $\text{Cu}_3(\text{dpa})_4\text{Cl}_2$ and related compounds: Bénard, M.; Berry, J. F.; Cotton, F. A.; Gaudin, C.; López, X.; Murillo, C. A.; Rohmer, M.-M. *Inorg. Chem.* **2006**, *45*, 3932.

the 1,2-dichloroethane solution. Yield: 0.042 g (24%). IR (KBr) ν/cm^{-1} : 1138, 1107(S=O), 1581, 1537, 1428 (py). UV/vis (CH_2Cl_2) $\lambda_{\text{max}}/\text{nm}$ ($\epsilon/\text{dm}^3 \text{ mol}^{-1} \text{ cm}^{-1}$): 350 (7.31×10^4), 500 (4.05×10^3); 890 (1.90×10^3). MS(FAB) m/z : 1587 ($[\text{Ni}_4(\mu_4\text{-Tsdpda})_4]^+$). Anal. Calcd for $\text{C}_{68}\text{H}_{56}\text{BF}_4\text{N}_{16}\text{Ni}_4\text{O}_8\text{S}_4$: C, 48.76; H, 3.37; N, 13.38. Found: C, 48.05; H, 3.54; N, 13.65.

Preparation of $[\text{Ni}_4(\mu_4\text{-DAniDANy})_4]$ (4**).** $\text{H}_2\text{DAniDANy}$ (0.186 g, 0.5 mmol), $\text{Ni}(\text{OAc})_2 \cdot 4\text{H}_2\text{O}$ (0.250 g, 1.0 mmol), and naphthalene (20 g) were placed in an Erlenmeyer flask. The mixture was heated at 220 °C for 3 h. After cooling the mixture to 80 °C, hexane (100 mL) was added to dissolve naphthalene and the resulting precipitate was filtered out. The solid was extracted with 100 mL of CH_2Cl_2 . The red-brown solution is immediately concentrated to 30 mL and layered with hexane. After a few days, 0.061 g of red-brown crystal was obtained in 53% yield. IR (KBr) ν/cm^{-1} : 1612, 1534, 1500 (py). UV (CH_2Cl_2) $\lambda_{\text{max}}/\text{nm}$ ($\epsilon/\text{dm}^3 \text{ mol}^{-1} \text{ cm}^{-1}$): 261 (1.63×10^5), 345 (7.05×10^4); 400 (1.51×10^5), 650 (3.74×10^3). MS(FAB) m/z : 1715 ($[\text{Ni}_4(\mu_4\text{-DAniDANy})_4]^+$). Anal. Calcd for $\text{C}_{88}\text{H}_{72}\text{N}_{16}\text{Ni}_4\text{O}_8$: C, 61.58; H, 4.23; N, 13.06. Found: C, 61.01; H, 4.11; N, 13.51.

Summary and Conclusion

The synthesis and structural characterization of $[\text{Ni}_4(\mu_4\text{-Tsdpda})_4(\text{H}_2\text{O})_2]$ (**2**), $[\text{Ni}_4(\mu_4\text{-Tsdpda})_4](\text{BF}_4)$ (**3**⁺), and $[\text{Ni}_4(\mu_4\text{-DAniDANy})_4]$ (**4**) extends the relatively restricted family of even-numbered metal chains stabilized with ligands derived from the polypyridylamide or naphthyridylamide groups. It also provides an opportunity to investigate the electronic structure and the magnetic behavior of these complexes in comparison with the more documented series of $\text{M}_3(\text{dpa})_4\text{L}_2$ complexes. An important difference with the odd-numbered chains of metal atoms concerns the equatorial surrounding of the metallic centers. In standard polypyridylamide complexes, the environment of the metal centers is characterized by an alternation between four pyridyl nitrogens, always occurring at both ends of the chain, and four amido nitrogens. In the even-numbered chains, the pyridyl and the amido nitrogens are either equally distributed around each metal center, as in **2** and in the previously reported $\text{Ni}_4(\mu_4\text{-phdpda})_4$ (**1**), or exhibiting an inverse distribution, as in **4**, where the terminal nickels are surrounded with four amido ends. In that sense, the DAniDANy ligand extends to four metal atoms the situation already characterized in the trimetallic linear complexes of the dianionic 2,6-bis-(phenylamido)pyridine (BPAP) ligand.²⁴ Since amido ends are more basic and give rise to shorter metal–ligand bonds,

this change has obvious structural consequences. This different distribution of the nitrogen ligand ends also enlightens the intricate relationship between equatorial and axial coordination. It was indeed known that $[\text{M}_3(\text{BPAP})_4]^{2-}$ ($\text{M} = \text{Cr}, \text{Ni}$) have no axial ligation, as $\text{Ni}_4(\mu_4\text{-phdpda})_4$ (**1**).²⁴ The same is true for **4**. Structural, magnetic, and theoretical evidence correlates this lack of axial coordination with a diamagnetic ground state for the complex, with no metal–metal interaction. However, **2** exhibits axial coordination, together with a four-electron/two-center antiferromagnetic coupling involving the terminal nickel atoms, as in the series of odd-numbered nickel chains. The present study has shown that the antiferromagnetic ground state persists in the hypothetical $[\text{Ni}_4(\mu_4\text{-Tsdpda})_4]$ complex, at variance with the other tri- and tetranuclear complexes characterized free of axial ligands. For **1** and **4**, the nondiamagnetic configuration of lowest energy involves the *innermost* Ni atoms, and therefore remains resistant to axial ligation. The case of **2** could therefore be considered as an exception in the small group of even-numbered chains of Ni atoms, since the electron-withdrawing character of the sulfonyl substituents seemingly counteracts the basicity of the terminal amido ligands and restores the antiferromagnetic coupling between terminal atoms.

Acknowledgment. The authors thank the CNRS, the Ministère de l'Éducation et de la Recherche (Paris, France) and the National Science Council and the Ministry of Education of the Republic of China (Taiwan, R. O. C) for financial support. Calculations have been shared between the IDRIS (CNRS, Orsay, France) and the CINES (Montpellier, France) National Computer Centers, the CURRI (ULP, Strasbourg, France), and the NCHC (Taiwan, R. O. C.). X.L. is grateful to the Government of Spain for a postdoctoral fellowship (No. EX-2004-0113).

Supporting Information Available: Total energies; symmetry constraints; optimized Cartesian coordinates; Mulliken charges; and atomic spin populations obtained from DFT/UB3LYP calculations carried out on the ground states of **1'**, **2'**, **3'**, [**3'**]⁺, **4'**, on the lowest diamagnetic state of **3'**, and on the lowest quintet states of **1'** and **4'**. X-ray crystallographic files are available for complexes **2**· $2\text{H}_2\text{O} \cdot \text{ClCH}_2\text{CH}_2\text{Cl}$, [**3**](BF_4)· $5\text{ClCH}_2\text{CH}_2\text{Cl}$, and **4**· $9\text{CH}_2\text{Cl}_2$ in standard CIF format. This material is available free of charge via the Internet at <http://pubs.acs.org>.

IC0612505